ELSEVIER

Journal of Fluids and Structures 24 (2008) 212–230

JOURNAL OF FLUIDS AND STRUCTURES

www.elsevier.com/locate/jfs

Exact and numerical responses of a plate under a turbulent boundary layer excitation

S. De Rosa*, F. Franco

ælab-Acoustics and Vibration Laboratory, Dipartimento di Progettazione Aeronautica[1], Università degli Studi di Napoli "Federico II", Via Claudio 21, 80125 Napoli, Italy

Received 23 January 2006; accepted 29 July 2007
Available online 19 November 2007

Abstract

The aim of this paper is the analysis of the predictive capabilities of the deterministic methodologies when facing the problem of a plate excited by a stochastic pressure distribution due to a turbulent boundary layer (TBL). A full analytical solution has been assembled by considering a simply supported rectangular plate wetted on one side by a TBL. This reference exact solution, developed by using a standard separable variable model, has been used as test case for comparing the approximate solutions coming from the adoption of a numerical scheme by using discrete coordinates. The numerical algorithm has been built by using a standard finite element modal approach. The approximations introduced are thoroughly discussed and analysed; they refer to the meshing condition and the transformation of the distributed stochastic load. The application of a novel numerical procedure named as Asymptotical Scaled Modal Analysis is presented too. This innovative numerical scheme allows the analysis of the structural response of a generic plane operator in the whole frequency range, which is not always amenable by exact solutions; further and equally important, it is associated to a reduction of the computational cost. The work demonstrates that some numerical advances in the prediction of the random structural responses are feasible still using standard finite element modal inputs, without increasing the computational costs.

Keywords: Turbulent boundary layer; Stochastic response; Plate vibration

1. Introduction

The turbulent boundary layer (TBL) is one of the most important sources of vibration and noise in automotive, aerospace, and railway transportation. The stochastic pressure distribution associated with the turbulence is able to excite significantly the structural response and the related acoustic radiated power. The problem is intrinsically multidisciplinary since it involves the mechanical vibrations, the aerodynamics, and the external/internal acoustics.

The predictive methodologies can be roughly grouped into two different families. The first is represented by the *modal methods* in which commonly all the required operators are expanded by using the structural in vacuum and undamped mode shapes and natural frequencies. Improvements can be performed by accounting also the aeroelastic interaction

*Corresponding author.
E-mail address: sergio.derosa@unina.it (S. De Rosa).
[1]From January 1st, 2007, Dipartimento di Ingegneria Aerospaziale.

0889-9746/$ - see front matter © 2007 Elsevier Ltd. All rights reserved.
doi:10.1016/j.jfluidstructs.2007.07.007

Nomenclature

a	stream-wise plate length
A_{QjQk}	joint acceptance between the jth and kth modes, Eq. (8)
Area	plate area
Area$_i$	equivalent area in finite element approach; in case of homogenous mesh is Δx, Δy
b	cross-wise plate length
E	Young's modulus
f	excitation frequency
f_C	critical frequency
h	plate thickness
H_i	ith term of the diagonal structural transfer functions matrix for the plate in finite element approach
i	imaginary unit
j_x and j_y	running integers for identifying the mode (number of half-waves)
k_c	convective wavenumber
L_x	stream-wise correlation length
L_y	cross-stream-wise correlation length
n	plate flexural modal density
n_S	scaled plate flexural modal density
n_x and n_y	running integers for identifying the mode (number of half-waves)
$\mathbf{N}$	shape function vector in finite element approach
NE	number of finite elements
NG	number of solution points for the evaluation of the mean response or number of grid of the finite element mesh
NM	number of retained structural eigensolutions for evaluating the response
NM_S	number of retained scaled structural eigensolutions for evaluating the scaled response
p	pressure
$\mathbf{r}$	absolute distance vector: $\mathbf{r}(r_x, r_y)$
R	nondimensional metric response
S_{FF}	random load matrix in finite element approach
S_p	(auto) power spectral density of the wall pressure distribution due to the turbulent boundary layer
S_w	spectral density (auto power) of the plate displacement
$\bar{S}_W$	mean spectral density (auto power) of the plate displacement
S_Φ	modal random load matrix in finite element approach
U_∞	free stream (undisturbed) speed
U_c	convective speed ($U_C = k_C\, U_\infty$)
w	out-of-plane displacement of the plate
x	stream-wise reference axis
Δx	extension of each finite element in stream-wise direction
X_{pp}	cross-spectral density of the wall pressure distribution due to the turbulent boundary layer
X_w	cross-spectral density of the plate displacement
y	cross-wise reference axis
Δy	extension of each finite element in cross-stream wise direction
Z_j	plate dynamic impedance for the ith mode

Greek symbols

α_x	stream-wise correlation coefficient
α_y	cross-stream-wise correlation coefficient
β_C	convective constant ($U_c = \beta_C\, U_\infty$)
γ_j	generalised mass coefficient for the plate jth mode
Γ	geometrical function in the cross spectral density
η	structural damping factor
η_S	scaled structural damping factor
Θ	intermediate integrals

λ_B	plate flexural wavelength
λ_E	aerodynamic wavelength
Λ	intermediate integrals
μ	modal overlap factor
μ_S	scaled modal overlap factor
ν	Poisson's ratio
ξ_x	stream-wise separation distance
ξ_y	cross-wise separation distance
ρ	material density
σ	scaling coefficient
$\sigma_{\min}$	minimum value of the scaling coefficient
$\mathbf{\Phi}$	matrix of the modal shape in finite element modal approach
ψ_i	ith analytical mode shape of the plate, ith column vector belonging to $\mathbf{\Phi}$
ω	circular excitation frequency
ω_j	natural circular frequency of the jth mode

Matrix and complex operators

*	complex conjugate operator
T	transposition operator
H	Hermitian operator
Re(…)	Real part

and/or by using complex modal basis. The *energy methods* constitute the second group: the target is to obtain a spatially averaged representation of the structural (and acoustic) response.

For increasing values of the modal overlap factor (the product among excitation frequency, modal density and damping), the efficiency and the efficacy of the energy methods become undoubted: they are able to give the global response with the lowest computational costs.

At the same time, when the value of the modal overlap factor is less than unity, the response is still dominated by the well resonating modes and therefore the modal methods are still useful since they furnish a solution with local characteristics; the question is still open of which methodology is the better for closing the gap from low to high values of the modal overlap factors.

The main contribution of the present work is just aimed to explore a possible extension of the standard finite element modal approach for such a problem. In the specific literature, the work by Davies (1971), Skudrzyk (1968) and Dowell (1975) are still among the best references for the subject, since they present the overall problem in its intrinsic complexity. In the last decade, the most interesting works are those authored by Graham (1996a, b, 1997, 1998). They represent a fundamental contribution to a modern view of this research problem, since they highlight several topics: the sensitivity of the structural response to the principal design parameters, the possibility to get asymptotic values of the related mathematical operators and a comparison of the available models for the TBL, and the influence of the Mach number.

Further contributions can be found also in the work by Clark and Frampton (1997) and Frampton et al. (1996): they present a fully aero-acousto-elastic problem and the results are related to both the subsonic and supersonic range of the undisturbed flow.

More recently, very interesting contributions in search of innovative and fast solutions for the stochastic response of a plate has also been addressed by Birgersson et al. (2003) and Mazzoni (2003); relevant works are also due to Maury et al. (2002), Hambric et al. (2004) and Finnveden et al. (2005). The last two are the ideal references for the present work since their contents strictly addressed the problem of the applicability of the deterministic simulation (finite element and spectral finite element).

The application of a scaling procedure is also presented for obtaining mean structural response at computational costs lower than the standard ones. Only recently this technique has been theoretically framed by using the Energy Distribution Approach in Mace (2003), and it has been named Asymptotical Scaled Modal Analysis, ASMA. The details of ASMA are summarised in De Rosa et al. (2005).

Methods working specifically for more intermediate values of the modal overlap factor appeared in last decade and they have to be considered as bridge methods, for closing the gap between modal and energy approaches (Desmet, 1998).

The present work would represent a step for extending the above-mentioned literature towards a detailed analysis of the simulation and the measurement problems associated to the response of structures driven by TBL wall pressure distribution.

All the themes herein presented and discussed were fully developed under the European project E.N.A.B.L.E. (Environmental Noise Associated with TBL Excitation, G4RD-CT-2000-00223, 5th Framework EU Research). Four main work packages represented the core of the project, whose main targets were (i) to develop models for TBL wall pressure fluctuations; (ii) to develop innovative predictive methodologies; (iii) to experimentally measure the vibration and noise levels associated with the TBL by using wind tunnel and in-flight tests; (iv) to compare the method and the experimental results.

The topics herein contained mainly belong to the second target, while the discussion about the adequacy of the TBL model and the relative comparison with the experimental measurements will be left to specific papers to appear in future.

The state of the art about the subject before the starting of the E.N.A.B.L.E. project can be found in Cousin (1999); a summary of the overall authors' involvement in the project is in De Rosa et al. (2003a, b) and Schröder (2004).

It will be shown that ASMA is able to provide a cost-efficient technique for predicting the mean velocity response and the radiated sound power of a typical aircraft panel over a broad frequency range, and well above the panel aerodynamic coincidence frequency. It has to be underlined that a large part of the sound inwardly radiated by aircraft panels, under a TBL excitation, lies in the frequency range up to the aerodynamic coincidence frequency. Therefore, the benefits of using standard and scaled FEM could be mitigated for this specific application, also considering the pressurisation effect that increases by a given factor the panel's first natural frequencies. Nevertheless, the pertinent procedure based on a sequence of standard and scaled FEM models, can be very useful when working with real configurations (in which the plate has to be considered with the full set of stringers, frame, etc.) and/or new materials (composite).

Trade-off analyses can be accomplished in the whole frequency range of interest, since ASMA generates the structural and acoustic response from a standard finite element model.

The work is structured as follows. In Section 2, the analytical expansions for the plate response as a consequence of having selected a given TBL source model; the proper detail will be given to the source and the response characteristics. This development was thought as absolutely necessary since a reference solution is needed, that is a solution in which for the given mode shapes and natural frequencies it is possible to get an exact spectral response. Only with this reference solution, in which the acceptance integral is solved in closed form, it was possible to introduce and then to verify the approximations due to the finite element approach and the scaling procedure. In Section 3, adequate attention is paid to present the several formulations in which the finite element approach could be applied for coping with the specific problem, while Section 4 presents the scaling procedure and the scaled finite element model for overcoming the classical difficulty of reproducing the response above the coincidence excitation frequency. Section 5 presents the adopted test-case and the results coming from exact modal expansion, standard finite element, and scaled finite element approach together with specific comments and remarks aimed to highlight the specific possibilities offered by the scaling procedure. Specifically, Section 5.1 compares the original and scaled modal expansions, while in Section 5.2 the original and scaled finite element model results are compared versus the exact ones.

2. Analytical expansions for the plate response

2.1. The turbulent boundary layer

The second-order statistics of the wall pressure fluctuations beneath a fully developed TBL are modeled as a random process homogenous in space and stationary in time field and can be characterised by the cross-spectral density function:

$$X_{pp}(\boldsymbol{\xi};\omega) = \int_{-\infty}^{\infty} \langle p(\mathbf{r};t)\cdot p(\mathbf{r}+\boldsymbol{\xi};t+\tau)\rangle \exp^{-i\omega\tau}\,d\tau, \tag{1}$$

where the symbol $\langle\ \rangle$ denotes the statistical average.

The vector $\mathbf{r}$ measures the distance of a given point from the origin of the reference system, while the vector $\boldsymbol{\xi}$ is the (relative) vector measuring the distance among two given points. This function is complex and can be expressed as follows:

$$X_{pp}(\boldsymbol{\xi};\omega) = S_p(\omega)\Gamma(\boldsymbol{\xi};\omega), \tag{2}$$

that is by using the product of the (auto) power spectral density S_p, and a geometrical function Γ; both are frequency dependent. Γ represents the correlation between two points whose distance is ξ. According to Newland (1984), the square modulus of Γ is the well-known coherence function. The coherence is often intended simply as the modulus of Γ.

Corcos proposed a simplified formulation of the cross-spectral density in which the geometrical function Γ is given by the product of two simple functions, while a third function rules the phase dependency (Corcos, 1964, 1967).

With reference to a plane surface belonging to an xy plane, where x is the stream-wise direction, Fig. 1:

$$X_{pp}(\xi_x,\xi_y,\omega) = S_p(\omega)\exp\left(-\alpha_x\left|\frac{\omega\xi_x}{U_c}\right|\right)\exp\left(-\alpha_y\left|\frac{\omega\xi_y}{U_c}\right|\right)\exp\left(-\frac{\mathrm{i}\omega\xi_x}{U_c}\right). \tag{3}$$

Corcos proposed also models for the coherence lengths and the convection velocity:

$$L_x(\omega) = \frac{U_c}{\alpha_x\omega}, \quad L_y(\omega) = \frac{U_c}{\alpha_y\omega}, \tag{4}$$

$$\frac{U_c}{U_\infty} = \beta_C, \quad k_c = \frac{\omega}{U_c}. \tag{5}$$

The symbol β_C denotes the "convective constant" and k_c is the convective wavenumber. The coefficients α_x and α_y indicate the loss of coherence in longitudinal and transversal directions, respectively. For smooth walls, commonly used values are: $\alpha_x = 0.116$ and $\alpha_y = 0.7$ (Blake, 1986). Other fundamental and interesting forms of the spectrum are due to Efimtsov (1982), where improved expressions are also suggested for evaluating them. A summary is in the already cited work by Graham (1997).

Another clear writing of the cross-spectral density is

$$X_{pp}(\xi_x,\xi_y,\omega) = S_p(\omega)\exp\left[-\frac{|\xi_x|}{L_x(\omega)}\right]\exp\left[-\frac{|\xi_y|}{L_y(\omega)}\right]\exp(-\mathrm{i}k_c\xi_x). \tag{6}$$

The Corcos model here briefly recalled is among the simplest representations of the wall pressure distribution due to a TBL, since (i) the space variables are separated, (ii) the phase variation is only accounted along the stream-wise direction, (iii) all functions have the same exponential form, and (iv) it is independent from any couple of points and depends only on their distance.

The Corcos model is an empirical model and the coefficients α_x and α_y are determined from measurements of the spatial coherence between two points of the wall pressure fluctuations. One of the main limitations of the model is in the sub-convective region since it overpredicts the power spectrum of the excitation by 20–40 dB. It is accurate only in the convective region where the stream-wise and the convective wavenumber are close: this is enough for aeronautical applications in the subsonic compressible speed range.

Further, the Corcos model is strictly suitable for the flow-induced noise prediction at very low frequencies since the correlation lengths, Eq. (4), should be bounded by the boundary layer thickness through a correcting factor (Efimtsov, 1982). However, Corcos suggested a convenient model due to its mathematical simplicity which allows closed-form expressions to be derived for the panel response.

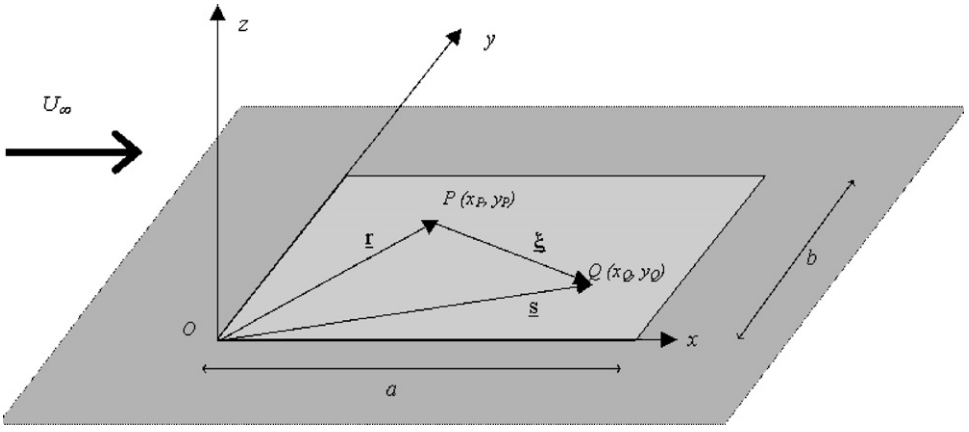

Fig. 1. Sketch of the elastic plate (light grey area) in the rigid aerodynamic baffle (dark grey area).

2.2. The plate response

The plate is thin, flat, rectangular and isotropic with no pre-stress (no pressurisation and no edge loadings). The plate is simply supported on all four edges. It is mounted in an infinite rigid plane baffle flush with the TBL, Fig. 1. The plate lies in an xy plane, and the flexural out-of-plane displacements, named $w(x,y,t)$, are along the z axis. The flow is along the x-axis.

The plate side lengths are a and b, in the stream-wise and cross-wise directions, respectively. In the present analysis it is assumed that any fluid-loading effect on the structural dynamic response can be neglected. This is motivated by a simple aeroelastic analysis in which it was verified that neither the natural frequencies nor the mode shapes are significantly modified when the case of the fluid wetting the plate is considered; this detail is not given here.

The displacement cross-spectral density between any arbitrary couple of points belonging to a thin, isotropic and homogenous plate, $A(x_A,y_A)$ and $B(x_B,y_B)$, due to an assigned stochastic distributed excitation, can be found with the following modal expansion as given in Elishakoff (1983):

$$X_w(x_A,y_A,x_B,y_B,\omega)=\sum_{j=1}^{\infty}\sum_{n=1}^{\infty}\left[\frac{\psi_j(x_A,y_A)\psi_n(x_B,y_B)}{Z_j^*(\omega)Z_n(\omega)}\right]\left[\frac{S_p(\omega)(ab)^2}{\gamma_j\gamma_n}\right]A_{Q_jQ_n}(\omega) \tag{7}$$

with

$$A_{Q_jQ_n}(\omega)=\int_0^a\int_0^a\int_0^b\int_0^b\left[\frac{X_{pp}(x,y,x',y',\omega)}{S_p(\omega)(ab)^2}\psi_j(x,y)\psi_n(x',y')\right]\mathrm{d}y\,\mathrm{d}y'\,\mathrm{d}x\,\mathrm{d}x'. \tag{8}$$

and

$$\gamma_j=\int_0^a\int_0^b\psi_j^2(x,y)\,\mathrm{d}y\,\mathrm{d}x,\quad Z_j(\omega)=\rho h\left[\omega_j^2-\omega^2+\mathrm{i}\eta\omega_j^2\right]. \tag{9}$$

The symbol ψ_i denotes the ith mode shape, and ω_i the ith natural radian frequency.

The integrals defined by the symbol A_{QjQk} are well known also as the acceptances: *joint acceptance* for $j=k$, or *cross acceptance* for $j\neq k$.

Further, the formulation contained in the Eqs. (7) and (8) can be applied to any structural operator once its modal base is known.

The auto-spectral density of the displacement at a selected point is given as follows:

$$\begin{aligned}S_w(x_A,y_A,\omega)&=\sum_{j=1}^{\infty}\sum_{n=1}^{\infty}\left[\frac{\psi_j(x_A,y_A)\psi_n(x_A,y_A)}{Z_j^*(\omega)Z_n(\omega)}\right]\left[\frac{S_p(\omega)}{\gamma_j\gamma_n}\right](ab)^2A_{Q_jQ_n}(\omega)\\&=\sum_{j=1}^{\infty}\left[\frac{\psi_j^2(x_A,y_A)}{|Z_j|^2\gamma_j^2}(ab)^2S_p(\omega)A_{Q_jQ_j}(\omega)\right]\\&\quad+2\,\mathrm{Re}\left\{\sum_{j=1}^{\infty}\sum_{n=j+1}^{\infty}\left[\frac{\psi_j(x_A,y_A)\psi_n(x_A,y_A)}{Z_j^*(\omega)Z_n(\omega)}\right]\frac{(ab)^2}{\gamma_j\gamma_n}\left[S_p(\omega)A_{Q_jQ_n}(\omega)\right]\right\}.\end{aligned} \tag{10}$$

It has to be noted that this last quantity is strictly real, as expected.

It should also be noted that it is possible to evaluate the plate mean response by using the following relationship:

$$\tilde{S}_W(\omega)=\frac{1}{\mathrm{Area}}\int_{\mathrm{Area}}S_W(x,y,\omega)\,\mathrm{d}x\,\mathrm{d}y. \tag{11}$$

This relationship reports the plate mean response in terms of displacement. For the orthogonality of the modes, it is simple to demonstrate that the modal cross terms do not give any contribution to this mean spectrum.

Similar quantities could be obtained by accepting an average over a selected number of points, NG:

$$\tilde{S}_W(\omega)=\frac{1}{NG}\sum_{i=1}^{NG}S_W(\omega,x_i,y_i). \tag{12}$$

The quantities presented in Eqs. (11) and (12) here have the same symbol but they will be well discriminated in the next paragraph. They can be named as continuous mean and discrete mean, respectively.

The number of the total modal components, NM, have to be selected in the expansions in order to achieve convergence of the results for the assigned excitation frequency.

These are the main quantities for a simply supported plate (Leissa, 1993):

(i) natural radian frequencies:

$$\omega_j = \sqrt{\frac{Eh^2}{12\rho(1-\nu^2)}}\left[\left(\frac{j_x\pi}{a}\right)^2 + \left(\frac{j_y\pi}{b}\right)^2\right]; \tag{13}$$

(ii) normalised mode shapes:

$$\psi_j(x,y) = \sin\left(\frac{j_x\pi x}{a}\right)\sin\left(\frac{j_y\pi y}{b}\right); \tag{14}$$

(iii) mode shape factor (generalised mass):

$$\gamma_j = \frac{ab}{4}; \tag{15}$$

(iv) acceptance for Corcos-like unit excitation:

$$A_{Q_jQ_n}(\omega) = \frac{1}{(ab)^2}\int_0^a\int_0^a\int_0^b\int_0^b \exp\left(-\frac{|\xi_x|}{L_x(\omega)}\right)\exp\left(-\frac{|\xi_y|}{L_y(\omega)}\right)\exp(-\mathrm{i}k_c\xi_x)\psi_j(x,y)\psi_n(x',y')\,\mathrm{d}y\,\mathrm{d}y'\,\mathrm{d}x\,\mathrm{d}x'. \tag{16}$$

The integral for the acceptances can be solved in closed form (see Appendix A), and the mean plate response in terms of displacement is given simply by

$$\tilde{S}_w(\omega) = \frac{1}{ab}\int_0^a\int_0^b S_w(x,y,\omega)\,\mathrm{d}y\,\mathrm{d}x = 4S_p(\omega)\sum_{j=1}^{NM}\frac{A_{Q_jQ_j}(\omega)}{|Z_j(\omega)|^2}. \tag{17}$$

At this point, an exact modal solution is available as reference for the comparison with any approximate methodology. This problem is amenable by an analytical solution in closed form since the TBL model uses separated space variables and functions with the same exponential form.

3. Finite element modal approach

It is evident that looking for the envisaged generalisation of the predictive procedure, a scheme in discrete coordinates, in order to take in account any configuration (material, shape, boundary conditions, etc.), must be pursued. A standard finite element solution has been assembled by using the following equation suitable for all the methods working with discrete coordinates (Elishakoff, 1983); the cross-spectral density matrix of displacements of a structural operator represented by using NG degrees of freedom and NM mode shapes is given by

$$\mathbf{S_W}(\omega) = \mathbf{\Phi H}(\omega)\mathbf{S_\Phi}(\omega)\mathbf{H}(\omega)^*\mathbf{\Phi}^{\mathrm{T}}, \tag{18}$$

with

$$\mathbf{S_\Phi}(\omega) = \mathbf{\Phi}^{\mathrm{T}}\mathbf{S_{FF}}(\omega)\mathbf{\Phi}, \tag{19}$$

where $\mathbf{\Phi}$ is the structural modal matrix (each column is an eigenvector sampled at the NG selected points), $[NG*NM]$; $\mathbf{H}(\omega)$ is the structural transfer function diagonal matrix, $H_j(\omega) = \left[\omega_j^2 - \omega + \mathrm{i}\eta\omega_j^2\right]^{-1}$, $[NM*NM]$; $\mathbf{S_\Phi}$ is the generalised force matrix, $[NM*NM]$; and $\mathbf{S_{FF}}$ is the equivalent force matrix, $[NG*NG]$.

There are two main problems associated with any approach using discrete representation. The first one is that the distributed random loads must be translated to this set of points. In the framework of the finite element method, the standard approach, named as *consistent*, is to use the shape function vector, $\mathbf{N_F}$, belonging to each element, as follows:

$$SC^{(E)}_{FF_{n,k}} = \int_{x_1^{(n)}}\int_{x_2^{(n)}}\int_{x_1^{(k)}}\int_{x_2^{(k)}} N_F^T X_{pp}\left(x_1^{(n)}, x_2^{(n)}, x_1^{(k)}, x_2^{(k)}, \omega\right) N_F\,\mathrm{d}x_1^{(n)}\,\mathrm{d}x_1^{(k)}\,\mathrm{d}x_2^{(n)}\,\mathrm{d}x_2^{(k)}. \tag{20}$$

The double integers n and k denotes here two generic finite elements, and the integration is related to the area of each of them. Accordingly, one gets the generic nkth member of the $NE \times NE$ matrix, where NE is the number of elements.

In this approach, the rotational degrees of freedom could be included too, for refining the evaluation. It should also be noted that the modal matrices are of $NE \times NE$ order.

A simplified approach refers to each grid point rather than each finite element. This means that the load acting on the ith grid point will be the resultant of the distributed load working on the equivalent nodal area, say Area_i, belonging to it. This area vector can be evaluated easily by using a static deterministic unit pressure load (De Rosa et al., 1994; Hambric et al., 2004).

Accordingly, one gets the generic ijth member of the $NG \times NG$ matrix:

$$SC_{FF_{i,j}}^{(G)} = \int_{x_i-\Delta x/2}^{x_i+\Delta x/2} \int_{x_j-\Delta x/2}^{x_j+\Delta x/2} \int_{y_i-\Delta y/2}^{y_i+\Delta y/2} \int_{y_j-\Delta y/2}^{y_j+\Delta y/2} X_{pp}(x_i, x_j, y_i, y_j, \omega)\, \mathrm{d}y_j\, \mathrm{d}y_i\, \mathrm{d}x_j\, \mathrm{d}x_i. \tag{21}$$

To both the points $P(x_i,y_i)$ and $Q(x_j,y_j)$ is assigned an area $\Delta x \Delta y$ and the double space integration refers to these finite domains.

A further approximation could also be introduced considering that the wall pressure distribution due to the TBL in the low frequency ranges does not fluctuate very quickly. In this case the last integral could be approximated as follows:

$$SL_{FF_{i,j}}^{(G)} = X_{pp}(x_i, x_j, y_i, y_j, \omega)[\Delta x \Delta y]^2. \tag{22}$$

Obviously, the approximations represented by Eqs. (20)–(22) are associated with decreasing computational costs. A summary of the approximations introduced are recalled and named in Table 1. Any of the three proposed approximations for assembling the load distribution, will always be represented by Hermitian operators, that is generically $(g)_{i,j} = (g)_{j,i}^*$. The C_1 and C_2 approximations have been tested but never used in the final calculations: the CPU time associated with their use was unacceptably high.

The second problem is associated to the wavelength discretisation. In fact, for the present model and assumptions, there are two characteristic wavelengths: one for the flexural waves travelling into the plate,

$$\lambda_B(\omega) = 2\pi \left(\frac{Eh^2}{12\rho\omega^2(1-\nu^2)} \right)^{1/4}, \tag{23}$$

and one associated to the flow speed,

$$\lambda_E(\omega) = \frac{2\pi}{k_c}. \tag{24}$$

The aerodynamic critical frequency is defined when the two wavelengths are equal, $\lambda_B = \lambda_E$; this holds at

$$f_c = \frac{U_c^2}{\pi h} \sqrt{\frac{3\rho(1-\nu^2)}{E}}. \tag{25}$$

This also means that a correct dynamic finite element model in any case cannot be used for $f > f_C$: for above coincidence frequency, the aerodynamic load is not correctly discretised by the F.E. mesh, therefore Eqs. (20)–(22) in any case gives a inconsistent result, Fig. 2. In the next paragraph these points will be better examined.

The discrete mean response of the structural operator could be defined as the average of the auto-spectra over all the available NG coordinates, Eq. (12). It has to be remembered that the central matrix of the product in Eq. (18), here named as $\mathbf{T}(\omega)$, $\mathbf{S_W}(\omega) = \mathbf{\Phi T}(\omega)\mathbf{\Phi}^{\mathrm{T}}$, is Hermitian, too.

The generic member is $T_{j,k} = H_j S_{\Phi_{j,k}} H_k^*$, and for the properties of the complex conjugate operator $T_{k,j} = H_k S_{\Phi_{k,j}} H_j^* = H_k S_{\Phi_{j,k,}}^* H_j^* = T_{j,k}^*$ also holds.

Table 1
List of approximations

Name	Approximations for $\mathbf{S_{FF}}$	Type/geometric reference	Equation
C_1	$\mathbf{SC}_{FF}^{(E)}$	Consistent/element	Eq. (20)
C_2	$\mathbf{SC}_{FF}^{(G)}$	Consistent/grid point	Eq. (21)
L_U	$\mathbf{SL}_{FF}^{(G)}$	Lumped/grid point	Eq. (22)

It should be noted also that

$$\mathbf{\Phi} = \begin{bmatrix} \Phi_1^{(1)} & \Phi_1^{(2)} & \cdots & \Phi_1^{(NM)} \\ \Phi_2^{(1)} & \Phi_2^{(2)} & \cdots & \Phi_2^{(NM)} \\ \vdots & \cdots & \ddots & \vdots \\ \Phi_{NG}^{(1)} & \Phi_{NG}^{(2)} & \cdots & \Phi_{NG}^{(NM)} \end{bmatrix} = \begin{bmatrix} \vec{\mathbf{\Phi}}^{(1)} & \vec{\mathbf{\Phi}}^{(2)} & \cdots & \vec{\mathbf{\Phi}}^{(NM)} \end{bmatrix}, \tag{26}$$

is always real by definition (the structural operator has been assembled by using a linear undamped model) and the eigenvectors represent an orthogonal base: $\vec{\mathbf{\Phi}}^{(j)} \cdot \vec{\mathbf{\Phi}}^{(k)} = 0$ with $j \neq k$.

Accordingly, the displacement auto-spectrum of the ith coordinate is given by

$$S_W(\omega)_{i,i} = \sum_{j=1}^{NM} \left[\Phi_i^{(j)}\right]^2 T_{j,j} + \sum_{k=1}^{NM} \sum_{j=1, j\neq k}^{NM} \Phi_i^{(j)} \Phi_i^{(k)} T_{j,k} = \sum_{j=1}^{NM} \left[\Phi_i^{(j)}\right]^2 T_{j,j} + 2 \sum_{k=1}^{NM} \sum_{j=k+1}^{NM} \Phi_i^{(j)} \Phi_i^{(k)} \mathrm{Re}(T_{j,k}). \tag{27}$$

This is a real quantity, as expected. By using the discrete mean, defined in Eq. (12) and imposing the orthogonality of the mode shapes in discrete coordinates, one gets

$$\bar{S}_W(\omega) = \frac{1}{NG} \sum_{i=1}^{NG} \left[\sum_{j=1}^{NM} \left(\Phi_i^{(j)}\right)^2 T_{j,j} \right] = \frac{1}{NG} \left[\sum_{j=1}^{NM} \left|\vec{\Phi}^{(j)}\right|^2 |H_j|^2 S_{\Phi_{j,j}} \right]. \tag{28}$$

The modal cross-terms do not give any contribution to the average quantities, as expected.

It has to be underlined that the average operation defined by Eq. (12) is not a unique possible choice. In discrete coordinates, it is possible to define an area discrete mean response:

$$\bar{S}_W(\omega) = \frac{1}{\mathrm{Area}} \sum_{i=1}^{NG} [S_W(\omega)]_i \mathrm{Area}_i. \tag{29}$$

In the case of a uniform mesh (all finite elements have the same geometry and dimensions) on a simply supported plate, and Eqs. (12) and (29) will furnish the same results. The same considerations hold for the continuous mean.

4. Scaled solutions: asymptotic scaled modal analysis

The scaling procedure is based on a simple consideration: the quadratic response depends on the number of modes resonating in a given frequency band, Ω, and on the damping. By modifying a given original modal base and accordingly the original damping, a scaled model has to be able to reproduce the quadratic response in the frequency range where enough modes are resonating. From the frequency range where $\mu \gg 1$, any quadratic response will be a

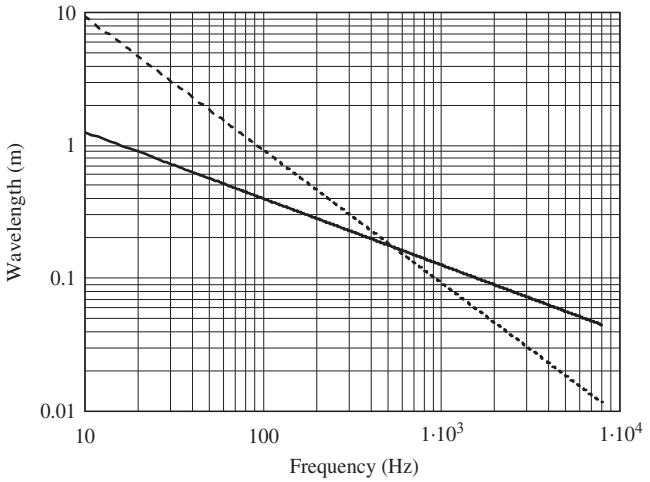

Fig. 2. Wavelengths (m) versus frequency (Hz): ——, structural; - - -, aerodynamic.

good estimator of the global response, and this can be obtained by using a low computational cost model since the scaling procedure allows using reduced spatial domains.

For the sake of completeness, the fundamental topics of the scaling procedure are briefly recalled (De Rosa et al., 1997; Franco et al., 1997).

All the linear dimensions, not involved in the structural energy transmission, have to be multiplied by a selected scaling coefficient, say σ (with $\sigma<1$). In the present problem, each side of the plate was scaled: $\bar{a}=\sigma a; \bar{b}=\sigma b$. Accordingly, the damping of the scaled model should be evaluated as

$$\bar{\eta}(\omega)=\frac{\eta(\omega)}{\sigma^2}. \tag{30}$$

All the mode shapes and natural frequencies will move to higher frequencies, for $\sigma<1$; for obtaining the same energy content, the original damping has to be accordingly augmented. This simple transformation generates a scaled system in which the energy representation (mean response) will be the same as the original system.

Preliminary analyses were also performed on a simplified equivalent problem (De Rosa et al., 2003c): a beam under a TBL excitation.

Recently, some new literature allowed framing the proposed approach from a theoretical point of view (Mace and Shorter, 2000; Mace, 2003) and further some applications are already available for simple and coupled plates (De Rosa et al., 2005).

The scaling procedure, now named ASMA (Asymptotic Scaled Modal Analysis) was also successfully verified with experimental measurements (Martini et al., 2004) and some insights can also be gained by using the statistical energy analysis, SEA, the more diffused technique for vibration and noise prediction at high values of modal overlap factors μ (Lyon, 1976).

The procedure can firstly be explained by using the principles of the SEA. Some details are given herein. For a generic plate, excited by a given input power Π_{IN}, the mean square velocity can be obtained as follows:

$$v^2_{\mathrm{SEA,I}}(\omega)=\frac{2\Pi_{IN}}{\rho a_I b_I h \eta_I \omega}. \tag{31}$$

For the sake of simplicity, a frequency-independent value of structural damping, η, has been supposed. The mean square velocity, $v^2_{\mathrm{SEA,I}}(\omega)$, is an average value taken over the spatial positions of the response and the excitation. A second flexural plate is now considered: it has different side lengths and damping; all the remaining parameters are left unaltered:

$$v^2_{\mathrm{SEA,II}}(\omega)=\frac{2\Pi_{IN}}{\rho a_{II} b_{II} h \eta_{II} \omega}. \tag{32}$$

The plate material and the thickness are not changed, i.e. the flexural wave speed is not changed either. It is simple to check that if $a_{II}=\sigma a_I$ and $b_{II}=\sigma b_I$, then

$$\eta_{\mathrm{II}}=\frac{\eta_{\mathrm{I}}}{\sigma^2}\hat{v}^2_{\mathrm{II}}(\omega)=\hat{v}^2_{\mathrm{I}}(\omega), \tag{33}$$

as anticipated.

The plate of reduced area ($\sigma<1$) will reproduce the same energy content by using an artificial damping obtained by accordingly increasing the original one. The application of the Energy Distribution Approach is more rigorous for explaining the ASMA and can be found in De Rosa et al. (2005).

It is simple to obtain that the modal overlap factors for the two flexural plates, original and scaled are equal:

$$\mu_{\mathrm{I}}(\omega)=\mu_{\mathrm{II}}(\omega). \tag{34}$$

In fact,

$$\begin{aligned} &a_S=\sigma a, \quad b_S=\sigma b, \quad \eta_S=\sigma^{-2}\eta\mu_S(\omega)=\omega\eta_S(\omega)n_S(\omega)=\mu(\omega),\\ &n(\omega)=\frac{1}{2\pi h}\frac{\sqrt{3}(ab)}{\sqrt{\dfrac{E}{\rho(1-\nu^2)}}}, \quad n_S(\omega)=\frac{1}{2\pi h}\frac{\sqrt{3}(a_S b_S)}{\sqrt{\dfrac{E}{\rho(1-\nu^2)}}}=\sigma^2 n(\omega). \end{aligned} \tag{35}$$

The (modal) deterministic simulation of the second plate will cost less than the first one: in fact, the flexural wavelength remains the same, but the domain is reduced; the spatial sampling, that is the number of needed solution points, will be reduced.

Any modal formulation could be applied on a reduced spatial domain, keeping unchanged the parameters involved in the energy transmission. It has to be well highlighted that the scaled models will be able to represent only the energy content, while the local information is completely lost.

The number of necessary modes for reaching the required convergence could also be kept or scaled too. It is simple to check that if NM are the modes needed for the original response in an assigned frequency band, the needed minimum number for the scaled modal base is $NM_S = NM\ \sigma^2$.

The scaling coefficient, σ, belongs to the range [0,1]: it is worth noting that for $\sigma = 1$ the scaled system equals the original. From a physical point of view, the lowest value to be assigned to σ should preserve the energy content of the original system.

A useful criterion has also been tested. It has been based on the ratio between the first natural frequencies of the system, damped and undamped (Skudrzyk, 1968). For the original and scaled system, the ratios are the following:

$$\kappa = \sqrt{1 - 2\left(\frac{\eta}{2}\right)^2}, \quad \kappa_S = \sqrt{1 - 2\left(\frac{\eta}{2\sigma^2}\right)^2}. \tag{36}$$

At this point an error function can be simply defined by accordingly comparing the last two expressions: $E = 1-(\kappa_S/\kappa)$. This error function depends on the original damping, as expected. For decreasing values of σ, the error function increases monotonically up to values that lead to unacceptable scaled representations.

It is useful to fix the error around 1%: the criterion allows using for a damping value of $\eta = 0.02$, $\sigma_{\min} \approx 0.30$; for an error of 5%, $\sigma_{\min} \approx 0.20$. By using values lower than this means that the scaled solution will spread the same energy content over too wide a frequency range.

Nevertheless, any possible criterion for defining the minimum value of the scaling factor should be physically related to the fact that the scaled structural damping cannot be too high. In fact, in that case the coupling between the models should be accounted and any uncoupled formulation, as Eq. (7), should not be pursued (Hasselman, 1976, 1977; Flax, 1977).

5. The test case and annotated results

Within the activities of the cited project ENABLE, a test case was defined among all its partners aimed to achieve an exact solution and methodological results. Here a summary is reported.

The wall pressure fluctuations were given by a Corcos model, Eq. (3), with the following set of parameters: $\alpha_x = 0.116$; $\alpha_y = 0.700$; $U_c = \beta_c U_\infty = 0.8$, $U_\infty = 92\,\mathrm{m/s}$. A nondimensional metric for the response of the plate was defined through the quantity R:

$$R(\omega) = \frac{\omega^4 (\rho h)^2 S_w}{S_p}. \tag{37}$$

The plate is simply supported on all four edges (implying separable sinusoidal mode shapes) and is mounted in an infinite rigid plane baffle, flush with the TBL. The particular plate is defined by the following choice of parameters: $a = 0.768\,\mathrm{m}$, $b = 0.328\,\mathrm{m}$, $h = 0.0016\,\mathrm{m}$, $E = 7 \times 10^{10}\,\mathrm{Pa}$, $\nu = 0.33$, $\rho = 2700\,\mathrm{kg\ m^{-3}}$. The structural damping (loss factor) of the plate, η, is assumed constant: $\eta = 0.02$.

For the specific values of the test, the previously defined critical frequency is $f_C = 537\,\mathrm{Hz}$.

The analytical and numerical structural responses have to be produced in different formats: the discrete mean over the four positions (Table 2) and the continuous mean.

5.1. Comparison of the analytical and scaled expansion responses

The first step was the generation of the analytical solution and to compare the different responses.

Fig. 3(a) just reports the analytical response for the selected test case by using the average response over the four positions of Table 2 and the mean response. The loss of the local characteristics for increasing excitation frequency is evident, that is for increasing values of the modal overlap factor. This last becomes unity at $f = 940\,\mathrm{Hz}$. For the sake of completeness, the unresolved spectral responses are reported in Fig. 3(b). They refer to each position of Table 2 and the continuous mean: the frequency range was restricted to 0–2 kHz to increase the readability of the figure. It has to be noted that the value on the left axis refers to a unit TBL spectrum, in view of subsequent normalisation as R, Eq. (37).

This result demonstrates that for $\mu > 1$ the quantity to be investigated can be a generic quadratic mean response rather than a specific kinematic response, as expected.

Table 2
The four positions for the plate response

	x (m)	y (m)
1	0.10	0.20
2	0.30	0.10
3	0.40	0.15
4	0.60	0.25

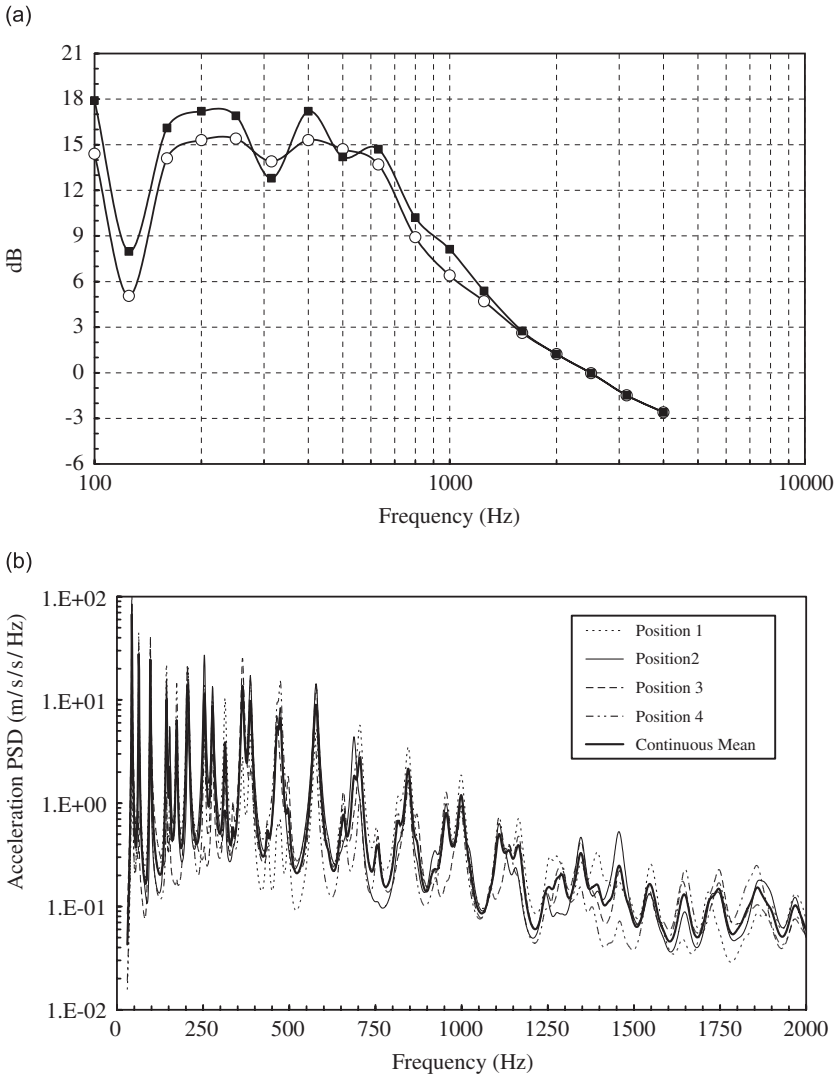

Fig. 3. (a) Metric R for the analytical responses of the plate: ○, continuous mean; ■, discrete mean. (b) Unresolved spectral responses, frequency step = 1 Hz.

It is also evident that the computational cost is much lower when working with the mean response. In the present results, Eqs. (10) and (12) were used in comparison with Eq. (11).

The solution has been generated by using 555 modes: the last resonating mode is at 18 kHz; this has been done for the sake of convergence in the response range 100–5000 Hz (in one-third octave bands).

The first interesting comparison has been obtained by applying the scaling procedure to the analytical solution as shown in Fig. 4: there, the discrete mean is reported and compared with analytical one. The analytical curve has been built by using 250 modes: they resonate in a frequency band 0–6 kHz, and the analysis was performed in the 0–2 kHz; the scaled one has been obtained with $\sigma = 0.5$ and by using only 60 modes. Fig. 4 shows that the scaled response is not able to reproduce the exact response when the modal overlap factor is still lower than unit value; it is expected to represent an acceptable approximation to the mean response, when this global estimator will be able to describe the plate response.

In Fig. 5 a comparison is just presented among the exact response, in terms of a continuous mean, and the scaled ones obtained by using the same analytical expansion but with the scaled plate (reduced side dimensions and increased damping). The scaled responses are reported in terms of the scaling coefficients. A better reading of Fig. 5 is achieved with the data of Table 3 where the percentage of the retained modes is specified, and further with the summary reported in Fig. 6 where a dB absolute error is plotted. This last is defined as follows:

$$\text{Error}(\omega, \sigma) = \left| 10 \log_{10} \left(\frac{\text{scaled response}}{\text{original response}} \right) \right|. \tag{38}$$

For the sake of precision, it has to be clarified that Fig. 6 shows the results averaged in a frequency band of 500 Hz, and the responses are generated from 2000 Hz, since the first natural frequency of the scaled plate with $\sigma = 0.15$ resonates at 1930 Hz.

All scaled models allow using only a small part of the original modes, even if this solution is associated to different errors. The criterion discussed in the fourth paragraph can be deduced from the content of the Fig. 6; in fact, a decreasing scaling coefficient is always associated with a reduction of the modal base, but the quality of the prediction begins to decrease too, since the modes are shifted to higher and higher frequencies, so that the value of $\sigma = 0.3$ can be considered an acceptable estimate of the inferior limit.

The model working with $\sigma = 0.35$ allows predicting the response within 0–2 dB error range in 2–10 kHz, by using only a limited fraction (16%) of the original eigensolutions.

This result in not surprising at all, since the response became global: only the proper modal density and the adequate modal overlap factor become the controlling parameters according to energy methods.

5.2. Comparison of the exact and numerical responses

At this point the finite element method was introduced in order to generalise the possible application of the techniques. The finite element solution uses a modal base generated by MSC/NASTRAN with a 4343 Grid Points model (101×43 mesh). The modal base was given as input to a FORTRAN code written for solving Eq. (28).

Fig. 7 reports a comparison of the analytical solution and the standard finite element solution. As expected, even if the mesh was built for simulating the structural wavelength up to 18 kHz, the solution is lost above the coincidence frequency.

Two items are confluent here. The first is that with the selected mesh the aerodynamic scales could be solved only up to 3 kHz; this can simply be checked by using the analysis of the aerodynamic wavelength, Fig. 2. The second is that the selected approximation, Eq. (22), further reduces the frequency range of validity of the proposed approach up to the critical aerodynamic frequency, as presented in Fig. 2. This specific problem could be solved by adopting two different meshing levels: one mesh for the structural domain and another for the aerodynamic field, as in a standard aeroelastic problem. This kind of approach is very expensive in terms of computational time because it involves an interpolation matrix between the structural domain and the aerodynamic one.

The same considerations of Fig. 4 can be made for Fig. 8, where now the scaled finite element response is presented. Again, the scaled finite element response is not able to reproduce the exact local response, but it is expected to represent an acceptable approximation to the mean response. A summary of the characteristics of the finite element models are in Table 4.

Some comments are needed for the analysis of the good results of Figs. 7 and 8.

The scaled procedure decreases by a factor σ the minimum flexural wavelength that can be predicted with the FEM. Above the coincidence region, the standard FEM diverges due to its inability to resolve the length scales of the order of the TBL correlation length, while the scaled FEM remains accurate since the minimum scaled flexural wavelength is still smaller than the lowest TBL correlation length (in the span-wise direction) at the limit of the upper frequency of interest, i.e. at 2 kHz. A criterion for the upper bound of the scaling procedure can be found just in this comparison between the predicted minimum flexural wavelength and the correlation lengths associated with the TBL. Roughly, for a generic deterministic excitation, the scaling model should work up to $1/\sigma$ times the original one, by keeping the original degrees of freedom.

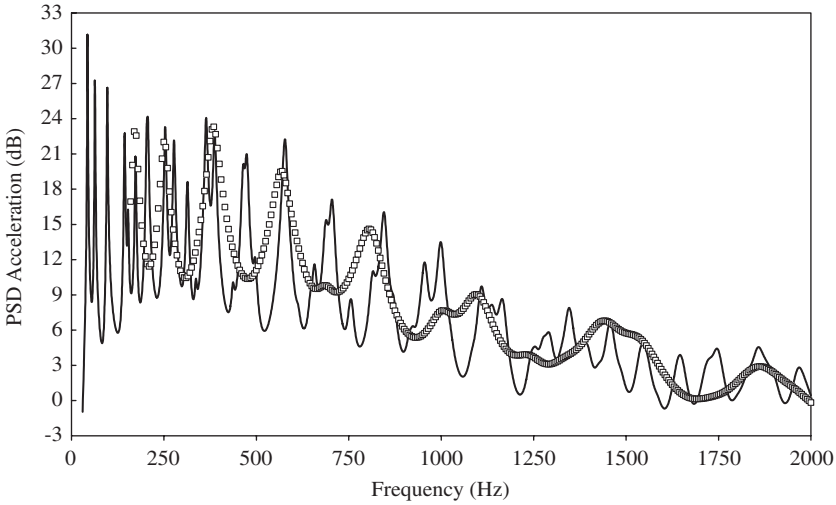

Fig. 4. Analytical and scaled analytical plate responses (discrete mean): ——, analytical; □, scaled analytical.

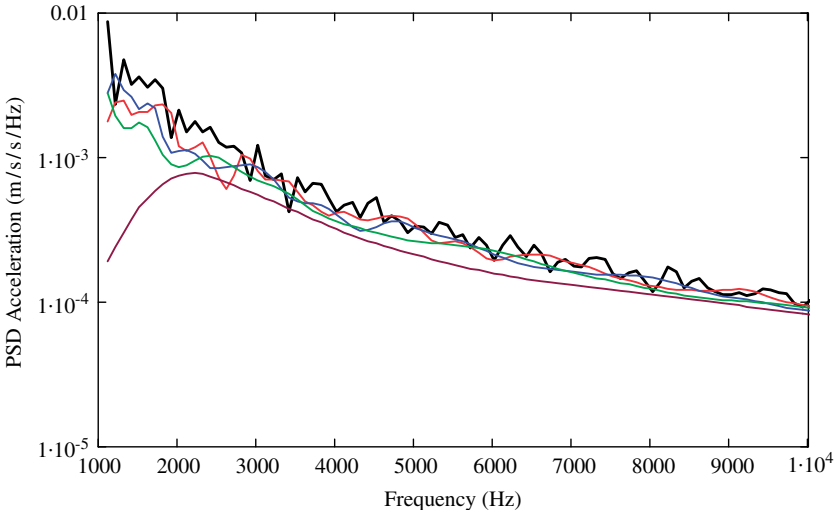

Fig. 5. Analytical and scaled expansion responses (continuous mean), $\Delta f = 100$ Hz: ——, analytical; ——, scaled $\sigma = 0.45$; —, scaled $\sigma = 0.35$; —, scaled $\sigma = 0.25$; —, scaled $\sigma = 0.15$. For interpretation of the references to the colour, the reader is referred to the web version of this article.

Table 3
Percentage of the modes used in the scaled expansion

σ	%	Modes
1.0	100	1392
0.45	24	334
0.35	16	223
0.25	7	97
0.15	3	42

Figs. 9 and 10 are the final results. They report the exact responses compared with those coming from the scaled finite element model in third octave frequency bands. Fig. 9 shows the discrete mean response (average responses over four positions) up to the 2 kHz centre frequency, by using 250 modes.

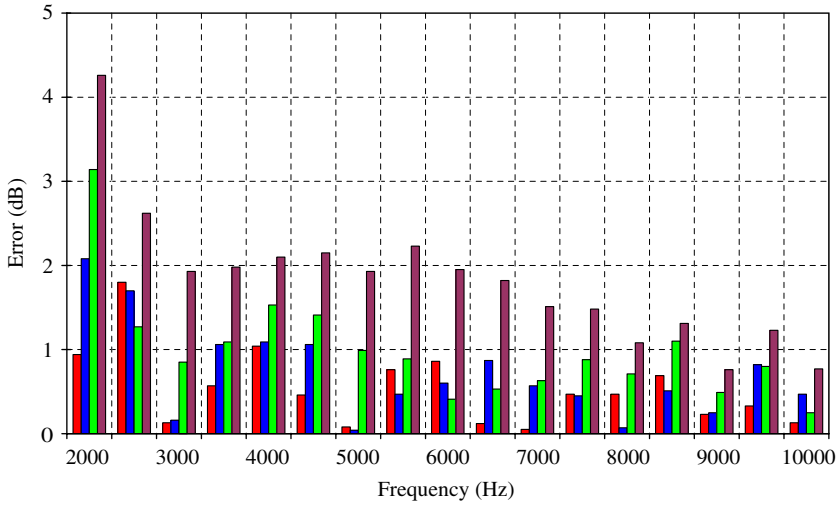

Fig. 6. Analytical and scaled expansion responses (continuous mean), averaged in frequency band, $\Delta f = 500$ Hz: ■, scaled $\sigma = 0.45$; ■, scaled $\sigma = 0.35$; ■, scaled $\sigma = 0.25$; ■, scaled $\sigma = 0.15$. For interpretation of the references to the colour, the reader is referred to the web version of this article.

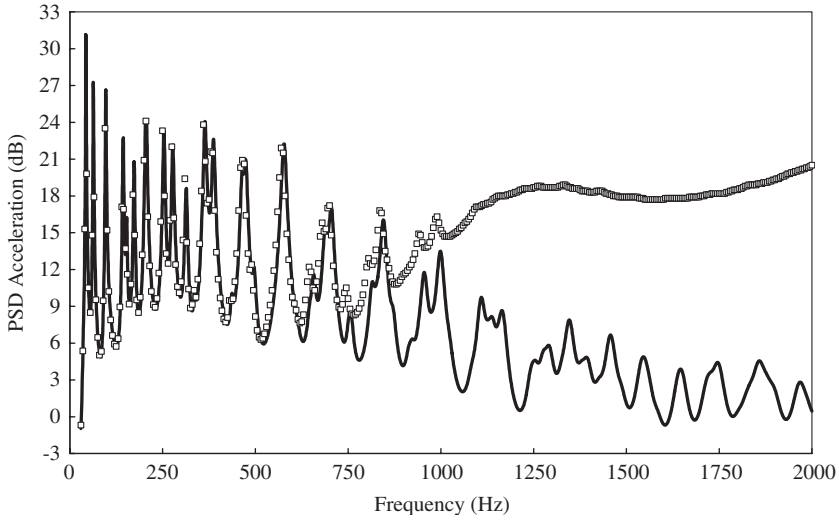

Fig. 7. Analytical and standard FEM plate responses (discrete mean): —, analytical; □, standard FEM.

Fig. 10 reports the continuous mean responses up to the 5 kHz centre frequency, by using 555 original modes and 44 scaled modes. For generating both the graphs, 20 samples for frequency band have been used. For the sake of completeness in Fig. 10 a predictive SEA curve has been added; it has been obtained with the standard SEA commercial code (AutoSEA2).

The scaling procedure keeps all the benefits of the standard FEM in solving complex materials, geometries and configurations.

Finally, a note on the time figures is necessary, since assuming a unit value (1 s) for the CPU time needed for getting the standard FEM mean response, the scaled FEM needs only 0.013 s: the scaling procedure is able to decrease the CPU time by two orders of magnitude. The CPU times for the local responses, that is for the discrete means, are not reported since for the scaled models they are meaningless. The CPU times for the Standard FEM have been used for comparison purposes even though, as extensively discussed, it is intrinsic inapplicable for above coincidence excitation frequencies.

Fig. 10 demonstrates that the scaled procedure is able to produce correct results with an acceptable computational cost in the above coincidence range and for values of the modal overlap factor greater than unity.

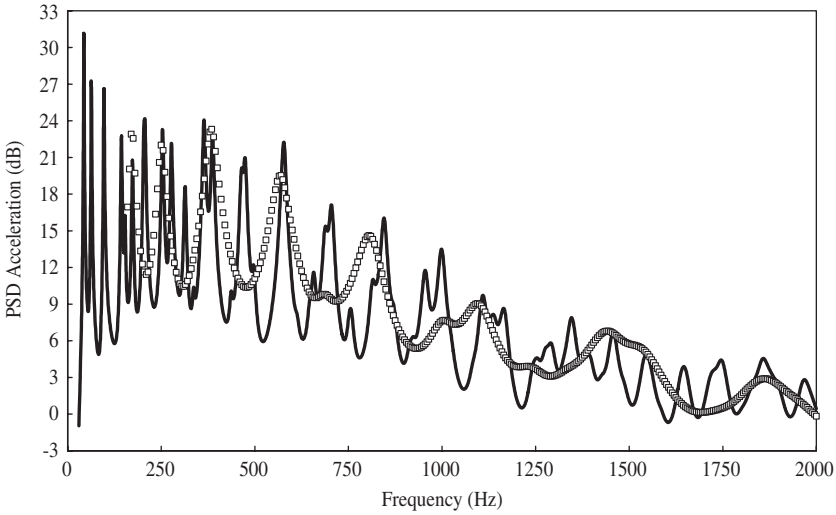

Fig. 8. Analytical and scaled FEM plate responses (discrete mean): —, analytical; □, scaled FEM.

Table 4
Summary of the finite element models

	Standard FEM	Scaled FEM
Number of grid points	4343 (101×43)	1122 (51×22)
Number of modes	188	44
Scaling coefficient	1.0	0.5
Used approximation	L_U (Table 1 and Eq. (22))	L_U (Table 1 and Eq. (22))

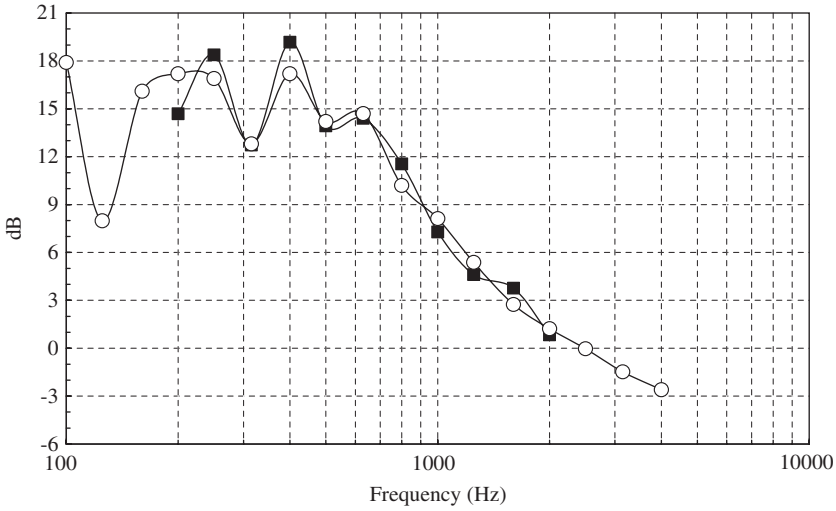

Fig. 9. Metric R (discrete mean) for the responses versus frequency ($\frac{1}{3}$ octave bands) (Hz): ○, exact; ■, scaled FEM.

The analysis of the more adequate TBL source model is not among the points addressed in the present work, but it has to be underlined that the discussed scaled procedure is able to work also with any model including the nonseparable variable ones.

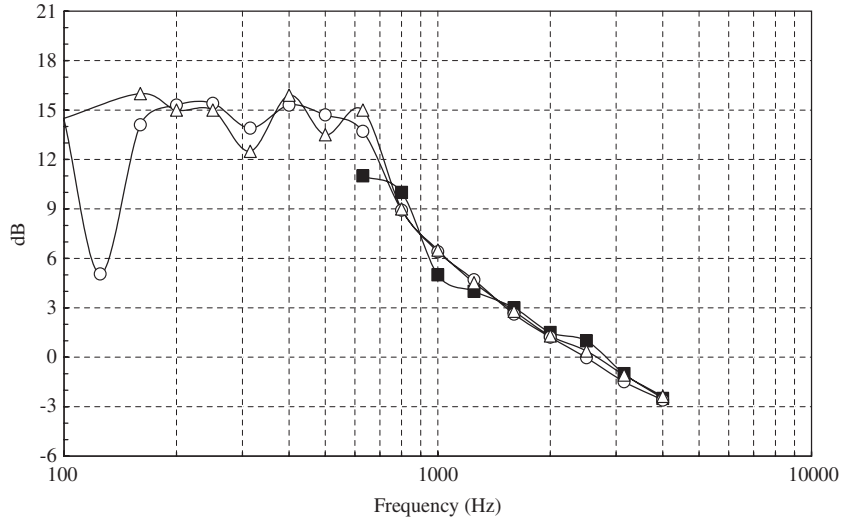

Fig. 10. Metric R for the responses versus frequency ($\frac{1}{3}$ octave bands) (Hz): ○, exact (continuous mean); ■, scaled FEM (continuous mean); △, SEA.

The effect of updating of the TBL source model and the analysis of the radiated acoustic power was already reported in De Rosa et al. (2003a, b) and Schröder (2004) always using the scaling procedure. The mentioned update was built by using the modifications proposed by Singer (1996) on the standard Corcos model.

The accuracy of ASMA was tested a few times with more complicated plate-edge conditions, since ASMA works well in the frequency range where the response is not dominated by the quality of the eigensolutions but only by their number; the analyst is then interested in the modal density, rather than identifying each single mode (and natural frequency). Further work is ongoing on built-up structures under both deterministic and random excitation.

6. Concluding remarks

The exact and predictive responses for a simply supported plate under a TBL excitation have been presented and discussed. The modal expansions have been used to obtain such a response, since this method well generalises the approach for more complicated structures and reproduces the standard finite element approach.

The choice of the Corcos model for the TBL distribution has been made only for keeping the simplicity of representation, even if this includes all the most important parameters of the TBL and although it has been evidenced that the modal approach could represent a solution to the predictive response even if the associated computational cost will become unacceptable.

A scaling procedure, named ASMA (Asymptotical Scaled Modal Analysis) has been so applied in order to overcome this problem. A computational domain has been defined by simply reducing the dimensions not involved in the energy transmission. The associated damping has been accordingly increased, in order to keep the same energy representation. The results are quite satisfactory.

ASMA has been successfully applied to both the exact modal expansion and a discrete coordinate solver, such as finite element based codes, and it led to a drastically strong reduction of the CPU time needed for obtaining the same frequency representation, overcoming at the same time the problem of the stochastic load representation in discrete coordinates at above coincidence frequencies.

Acknowledgements

This work has been firstly developed under the project ENABLE: "*Environmental Noise Associated with turbulent Boundary Layer Excitation*", EU Research Programme FP5, Contract No. G4RD-CT-2000-00223. The work was further partially supported by the *Italian Ministry of the Education, University and Research* (M.I.U.R.), through the

co-funded national research projects COFIN2003 and COFIN2005. Sincere thanks are for our colleague Prof. F. Marulo, the editor-in-chief, the associate editor and the anonymous referees: their remarkable comments, criticisms and suggestions greatly improved the original work.

Appendix A

The integral for the acceptances can be solved in closed form:

$$A_{Q_jQ_n}(\omega)=\frac{1}{(ab)^2}\int_0^a\int_0^a\int_0^b\int_0^b \exp\left(-\frac{|\xi_x|}{L_x(\omega)}\right)\exp\left(-\frac{|\xi_y|}{L_y(\omega)}\right)\exp(-\mathrm{i}k_c\xi_x)\psi_j(x,y)\psi_n(x',y')\,\mathrm{d}y\,\mathrm{d}y'\,\mathrm{d}x\,\mathrm{d}x'. \tag{A.1}$$

According to the given model for the TBL (separable variables), the integral of the joint acceptance can be split along the two reference directions:

$$A_{Q_jQ_n}(\omega)=\Lambda_{Q_jQ_n}(\omega)\Theta_{Q_jQ_n}(\omega), \tag{A.2}$$

with

$$\begin{aligned}\Theta_{Q_jQ_n}(\omega)&=\frac{1}{b^2}\int_0^b\int_0^b \sin\left(\frac{j_y\pi y}{b}\right)\sin\left(\frac{n_y\pi y'}{b}\right)\exp\left(-\frac{|\xi_y|}{L_y(\omega)}\right)\mathrm{d}y\,\mathrm{d}y',\\ \Lambda_{Q_jQ_n}(\omega)&=\frac{1}{a^2}\int_0^a\int_0^a \sin\left(\frac{j_x\pi x}{a}\right)\sin\left(\frac{n_x\pi x'}{a}\right)\exp\left(-\frac{|\xi_x|}{L_x(\omega)}\right)\exp(-\mathrm{i}k_c\xi_x)\,\mathrm{d}x\,\mathrm{d}x'.\end{aligned} \tag{A.3}$$

Each of the previous integrals can be analysed in a general form (Elishakoff, 1983)

$$I_{jn}(\omega)=\int_0^L\int_0^L \Omega(x_2-x_1,\omega)\vartheta_j(x_1)\vartheta_n(x_2)\,\mathrm{d}x_1\,\mathrm{d}x_2. \tag{A.4}$$

A transformation of the variables and accordingly of the integration domain leads to this other form:

$$\begin{aligned}\bar{K}_{jn}(\omega,\xi)&=\int_{\xi/2}^{L-\xi/2}\vartheta_j\left(\eta-\frac{\xi}{2}\right)\vartheta_n\left(\eta+\frac{\xi}{2}\right)\mathrm{d}\eta,\quad \bar{\bar{K}}_{jn}(\omega,\xi)=\int_{\xi/2}^{L-\xi/2}\vartheta_j\left(\eta+\frac{\xi}{2}\right)\vartheta_n\left(\eta-\frac{\xi}{2}\right)\mathrm{d}\eta,\\ I_{jn}(\omega)&=\int_0^L\Omega(\xi,\omega)\bar{K}_{jn}(\omega,\xi)\,\mathrm{d}\xi+\int_0^L\Omega(-\xi,\omega)\bar{\bar{K}}_{jn}(\omega,\xi)\,\mathrm{d}\xi.\end{aligned} \tag{A.5}$$

An exact solution in closed form can be found for the integrals in Eq. (A.5), thus leading to an explicit expression for each member of the product of integrals defined in Eq. (A.2). The given model for the TBL (separable variables) also leads to

$$A_{Q_jQ_n}(\omega)=A^*_{Q_nQ_j}(\omega). \tag{A.6}$$

References

Birgersson, F., Ferguson, N.S., Finnveden, S., 2003. Application of the spectral finite element method to turbulent boundary layer induced vibration of plates. Journal of Sound and Vibration 259, 873–891.

Blake, W.K., 1986. Mechanics of Flow-Induced Sound and Vibration, Vol. II. Academic Press, New York.

Corcos, G.M., 1964. The structure of the turbulent pressure field in boundary-layer flows. Journal of Fluid Mechanics 18, 353–379.

Corcos, G.M., 1967. The resolution of turbulent pressure at the wall of a boundary layer. Journal of Sound and Vibration 6, 59–70.

Cousin, G., 1999. Sound from TBL induced vibrations. Doctoral Thesis, KTH Marcus Wallenberg Laboratory for Sound and Vibration Research, Stockholm, Sweden, ISSN 1103-470X.

Davies, H.G., 1971. Sound from turbulent boundary layer excited panels. Journal of the Acoustical Society of America 49 (Part II), 878–889.

De Rosa, S., Pezzullo, G., Lecce, L., Marulo, F., 1994. Structural acoustic calculations in the low frequency range. AIAA Journal of Aircraft 31, 1387–1394.

De Rosa, S., Franco, F., Ricci, F., Marulo, F., 1997. First assessment of the energy based similitude for the evaluation of the damped structural response. Journal of Sound and Vibration 204, 540–548.

De Rosa, S., Franco, F., Melluso, D., 2003a. Analysis of radiated power from a plate in a turbulent boundary layer. Invited Paper at Euronoise Conference 2003, Naples, Italy, p. 47.

De Rosa, S., Franco, F., Melluso, D., 2003b. The analysis of the stochastic response of plates: a review of the project E.N.A.B.L.E. XVII A.I.D.A.A. In: National Congress of the Italian Association for Aeronautics and Astronautics, Rome, Italy, pp. 167–176.

De Rosa, S., Franco, F., Romano, G., Scaramuzzino, F., 2003c. The random structural response due to a turbulent boundary layer excitation. Wind and Structures 6, 437–450.

De Rosa, S., Franco, F., Mace, B.R., 2005. The asymptotic scaled modal analysis for the response of a two plate assembly. In: XVIII AIDAA National Congress, 19–22 Sept., Volterra (PI), Italy.

Desmet, W., 1998. A wave based prediction technique for coupled vibroacoustic analysis, Ph.D. Dissertation. KUL, Leuven, Belgium.

Dowell, E.H., 1975. Aeroelasticity of Plates and Shells. Noordhoff International Publishing, Leyden, The Nederlands.

Efimtsov, B.M., 1982. Characteristics of the field of turbulent wall pressure fluctuations at large Reynolds numbers. Soviet Physics Acoustics 28, 289–292.

Elishakoff, I., 1983. Probabilistic Methods in the Theory of Structures. Wiley, New York.

Finnveden, S., Birgersson, F., Ross, U., Kremer, T., 2005. A model of wall pressure correlation for prediction of turbulence-induced vibration. Journal of Fluids and Structures 20, 1127–1143.

Flax, A.H., 1977. Comment on "Modal coupling in lightly damped structures". AIAA Journal 15, 1662.

Frampton, D., Clark, R.L., Dowell, E.H., 1996. State-space modeling for aeroelastic panels with linearized potential flow aerodynamic loading. AIAA Journal of Aircraft 33, 816–822.

Franco, F., et al., 1997. The energy based similitude for the energetic vibration response prediction of 2D systems. Confederation of European Space Agencies (C.E.A.S.) International Forum on Structural Dynamics and Aeroelasticity, vol. III, Rome-IT, pp. 223–229.

Graham, W.R., 1996. Boundary layer induced noise in aircraft, Part I, the flat plate model. Journal of Sound and Vibration 192, 101–120.

Graham, W.R., 1996. Boundary layer induced noise in aircraft, Part II, the trimmed flat plate model. Journal of Sound and Vibration 192, 121–138.

Graham, W.R., 1997. A comparison of models for the wavenumber frequency spectrum of turbulent boundary layer pressures. Journal of Sound and Vibration 206, 541–565.

Graham, W.R., 1998. The effect of the mean flow on the radiation efficiency of rectangular plates. Proceedings of the Royal Society of London A 454, 111–137.

Hambric, S.A., et al., 2004. Vibrations of plates with clamped and free edges excited by low-speed turbulent boundary layer flow. Journal of Fluids and Structures 19, 93–110.

Hasselman, T.K., 1976. Modal coupling in lightly damped structures. AIAA Journal 14, 1627–1628.

Hasselman, T.K., 1977. Reply by Author to A.H. Flax. AIAA Journal 15, 1662–1663.

Leissa, A.L., 1993. Vibrations of Plates. Published for the Acoustical Society of America through the American Institute of Physics.

Lyon, R.H., 1976. Statistical Energy Analysis of Dynamical Systems: Theory and Applications. MIT Press, Cambridge, MA.

Mace, B.R., 2003. Statistical energy analysis, energy distribution models and system modes. Journal of Sound and Vibration 264, 391–409.

Mace, B.R., Shorter, P.J., 2000. Energy flow models from finite element analysis. Journal of Sound and Vibration 233, 369–389.

Martini, L., De Rosa, S., Franco, F., 2004. The structural response of a three plate assembly. In: International Conference on Noise and Vibration Engineering ISMA2004, Leuven BE, paper 336.

Maury, C., Gardonio, P., Elliott, S.J., 2002. A wavenumber approach to modelling the response of a randomly excited panel, Part II: application to aircraft panels excited by a turbulent boundary layer. Journal of Sound and Vibration 252, 115–139.

Mazzoni, D., 2003. An efficient approximation for the vibro-acoustic response of a turbulent boundary layer excited panel. Journal of Sound and Vibration 264, 951–971.

Newland, D.E., 1984. An Introduction to Random Vibration and Spectral Analysis. Longman, New York.

Schröder, W., 2004. Aeroacoustics research in Europe: the CEAS-ASC report on 2003 highlights. Journal of Sound and Vibration 278, 1–19.

Singer, B.A., 1996. Turbulent wall pressure fluctuations: new model for off axis cross spectral density. NASA CR 198297.

Skudrzyk, E., 1968. Simple and Complex Vibratory Systems. The Pennsylvania State University Press, University Park, London.